EARTH SURFACE PROCESSES AND LANDFORMS
Earth Surf. Process. Landforms **41**, 587–602 (2016)

Published online 16 November 2015 in Wiley Online Library
(wileyonlinelibrary.com) DOI: 10.1002/esp.3847

Insights into rock avalanche emplacement processes from detailed morpho-lithological studies of the Tschirgant deposit (Tyrol, Austria)

Anja Dufresne,[1]* Christoph Prager[2,3] and Annette Bösmeier[4]
[1] Geologie, Universität Freiburg, Freiburg, Germany
[2] alpS GmbH, Innsbruck, Austria
[3] ILF Consulting Engineers Austria GmbH, Innsbruck, Austria
[4] Geographie, Universität Freiburg, Freiburg, Germany

Received 18 June 2015; Revised 3 October 2015; Accepted 5 October 2015

*Correspondence to: Anja Dufresne, Geologie, Universität Freiburg, Freiburg, Germany. E-mail: volcanja@web.de

ESPL
Earth Surface Processes and Landforms

ABSTRACT: Large, rapid rockslope failures generate deposits with complex morphologies due to a number of causal and influencing factors. To investigate these, we conducted a detailed case study at the carbonate Tschirgant deposit (Tyrol, Austria). It preserved evidence of simultaneous rock sliding (very large, coherent hummocks) and rock avalanche spreading (smaller, more scattered hummocks and ridges). Motion indicators, such as longitudinal ridges furthermore pinpoint the transition between linear sliding and radial spreading. The lithological distribution in the Tschirgant deposit shows that it retained source stratigraphy despite being split into two accumulation lobes by a high bedrock ridge. Furthermore, lithology had a very strong control on the final deposit morphology in that the different lithologic units form individual deposit surfaces. River erosion has created fortuitous outcrops that reveal the basal rock avalanche contact. The underlying valley-fill sediments (substrates) have been intricately involved in shaping the rock avalanche morphology and, where entrained, highlight internal rock avalanche deformation features. This study shows that intrinsic dynamic properties of granular media (e.g. tendency for longitudinal alignments), emplacement mode, lithology (and source predisposition), runout path topography, and substrates form the quintet of causal factors that shape rock avalanche morphology.

KEYWORDS: rock avalanche; rockslide; carbonates; emplacement processes; deposit morphology

Introduction

Hummocky landforms have long attracted scientific interest. In some mountain regions, such deposits have undergone a substantial shift in interpretation from climate-indicative glacial deposits into singular, catastrophic rockslope failure events (Hewitt, 1999; Hewitt *et al.*, 2008; McColl and Davies, 2011; Robinson *et al.*, 2014). Furthermore, since the cataclysmic eruption and sector collapse of Mt St Helens volcano in Washington, USA in 1980 (e.g. Glicken, 1996), hummocky deposits in volcanic regions have also been reinterpreted as end products of catastrophic rather than glacial processes.

Rock avalanches result from sudden failure of rock slopes. They translate great masses ($> 10^6$ m^3) of crushing and pulverizing dry rock at high velocities (50–150 m/s; Heim 1932) and bury tens of square kilometres of land under tens of meters thick debris. It is this streaming nature that is alluded to by the term 'avalanche' (German 'Sturzstrom'; Heim, 1932; Hsü, 1975; Erismann and Abele, 2001). Runout distances of several kilometres exceed those predicted by simple frictional models, invoking emplacement theories that are discussed at length in the literature (e.g. Erismann and Abele, 2001; Legros, 2002). Their catastrophic nature and dust clouds rising high above the streaming debris exclude direct observation of their emplacement processes. We thus rely on the morphological, structural, and sedimentological features preserved in the final deposit. Field observations and literature accounts present a number of features observed at rock and debris avalanche deposits worldwide. For example, hummocks (hills or hillocks of various shapes), toma hills (isolated conical mounds or steep hills), ridges (Ampferer, 1904; Heim, 1932; Abele, 1972, 1974), and flowbands are common surface expressions of dry granular flows – from the very large (10^6–10^9 m^3) rock and volcanic debris avalanches (e.g. Siebert, 2002; Yoshida *et al.*, 2012) down to very small laboratory experiments (cm^3; e.g. Pouliquen *et al.*, 1997; Dufresne and Davies, 2009; Paguican *et al.*, 2014). In unobstructed runout, hummock sizes tend to decrease and their number to increase with distance travelled (e.g. Yoshida *et al.*, 2012; Paguican *et al.*, 2014, and references cited therein). Furthermore, hummock and ridge alignment is typically radial with respect to their point of origin (Dufresne *et al.*, 2010; McColl and Davies, 2011). Ridges can evolve into much thinner and longer flowbands signalling high mobility (McSaveney, 1978; Naranjo and Francis, 1987; Dufresne and Davies 2009). Hewitt *et al.* (2008) stated that simple, unimpeded rock avalanches form extensive, thin (2–10 m), and

lobate deposits (e.g. Frank Slide, Canada), but also that few such cases exist. As soon as rising topography, retarding basal conditions or partial slowing of frontal avalanche material is encountered, hummocks seem to merge, or coalesce to form larger structures (compound hummocks; e.g. Clavero *et al.*, 2004). Hummock long-axes in many obstructed settings are oriented (sub-)perpendicular to motion direction (Heim, 1932; Abele, 1972, 1974, 1997; Prager *et al.*, 2006). An alternative mechanism on the formation of distal, transverse ridges was put forward by Ostermann *et al.* (2012 p. 91), wherein 'surging, i.e. fluctuations of both velocity and thickness of a flow associated with downflow propagation of roll waves' is proposed. Distinct horst-and-graben structures can be produced in extensional spreading by pull-apart mechanisms (Abele, 1997; Xu *et al.*, 2012). Many authors observed that the deposits of rock avalanches, rockslides, and volcanic debris avalanches retain the stratigraphic sequence of their source slopes (Heim, 1932; Johnson, 1978; Yarnold and Lombard, 1989; Vallance *et al.*, 1995; Capra *et al.*, 2002; Abdrakhmatov and Strom, 2006; Geertsema *et al.*, 2006; Hewitt *et al.*, 2008; Dufresne *et al.*, 2009; Weidinger *et al.*, 2014). Additionally, preparatory conditions at the source dictate, for example, the maximum clast size for any given unit in the final deposit. In most cases, the deposit surface is covered with an open network of large angular boulders, the carapace (Heim, 1932; Abele, 1974; Sørensen and Bauer, 2003; Prager, 2010; Davies and McSaveney, 2012).

Any emplacement hypothesis must withstand the test of, i.e. match these field observations. Our objectives are therefore to identify the morphometric signatures unique to particular emplacement processes and runout path conditions through the combination of morphometric analyses of high-resolution LiDAR (light detection and ranging) images and detailed field mapping. We present a new, highly detailed case study of the apparently very complex Tschirgant rock avalanche deposit in Tyrol, Austria. The following reasons make it an ideal site for these detailed investigations. Its main mass is largely monolithologic (carbonates), but contains stratigraphic 'marker beds' that enable field mapping of the lithological distribution and the assessment of the influence of different mechanical rock mass properties. The runout path provides diverse topographic settings. The contact zone of landslide deposits and underlying valley floor sediments is naturally exposed. High-resolution LiDAR images are available and show the presence of all the aforementioned deposit surface features. Finally, some borehole data (tiris, https://portal.tirol.gv.at) provide information about deposit thickness and grain size distributions.

Study Site and Methods

Geologic setting

Situated at the southern margin of the Northern Calcareous Alps, a major Austroalpine thrust complex, the Tschirgant ridge (Figure 1) comprises a stacked nappe pile of Lower to Upper Triassic shallow marine carbonates that were affected by complex fold and fault systems (Ampferer, 1904, 1905; Grottenthaler, 1968; Brandner, 1980; Niederbacher, 1982; Eisbacher and Brandner, 1995; Pagliarini, 2008; Geofast, 2011).

The well-exposed rock avalanche scarp (Weißwand, Figure 1), with its top at 2160 m above sea level (a.s.l.), is characterized by massive to thick-bedded, intensively fractured limestones and dolostones of the Wetterstein Formation in contact with well-bedded carbonates of the Alpine Muschelkalk Group (Figure 2). Lower sections of the failed slope comprise less competent bedrocks, i.e. the characteristic alternations of three siliciclastic and carbonate sequences of the Raibl Group (see Tollmann, 1976). These clay, silt and sandstones (anchi-metamorphic, herein termed 'clayshales'), dolostones, limestones and cellular carbonates/evaporates (German: 'rauhwacken') are distinct rock types that can be well-mapped at both the scarp and in the accumulation area of the Tschirgant landslide. Hauptdolomit, a lithologically rather monotonous sequence of decimetre to metre bedded, dark grey microcrystalline and sometimes bituminous dolomites (Tollmann, 1976; Fruth and Scherreiks, 1982; Brandner and Poleschinski, 1986; Donofrio *et al.*, 2003) is present at the lower parts of the Tschirgant ridge. The structural setting is characterized by complex patterns of ENE-WSW striking main fold and fault systems, and NW-SE and NE-SW striking strike-slip faults (Eisbacher and Brandner, 1995; Pagliarini,

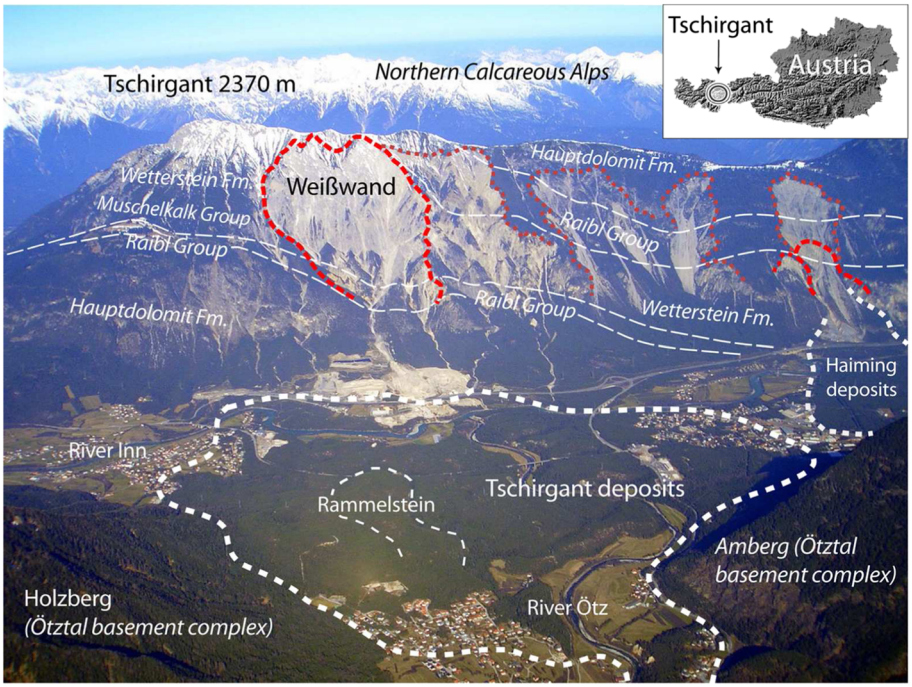

Figure 1. Tschirgant rock avalanche scarp and accumulation area, depicting main geological units and locations (see text). Prager *et al.*, 2008, modified; oblique air photograph courtesy of M. Schuster (2007). This figure is available in colour online at wileyonlinelibrary.com/journal/espl

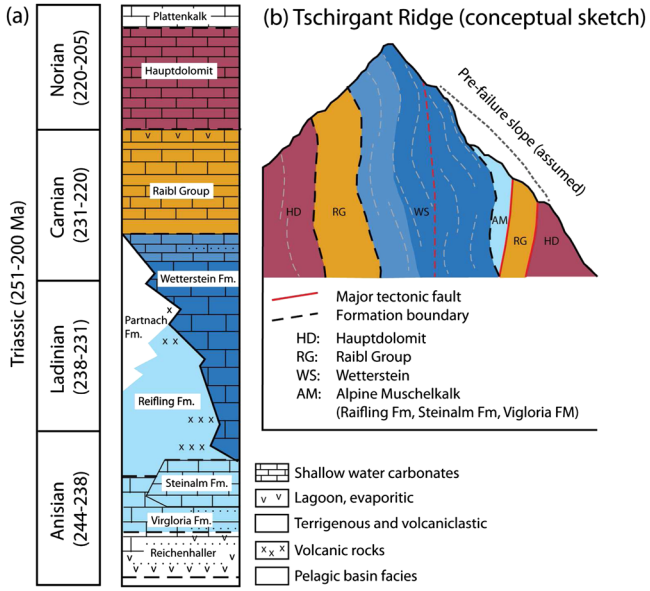

Figure 2. Stratigraphic profile of the source bedrock lithologies (modified after Brandner, 1984) with the units found in the Tschirgant rock avalanche deposit and their arrangement in the Tschirgant ridge (after Prager *et al.*, 2007; Pagliarini, 2008). This figure is available in colour online at wileyonlinelibrary.com/journal/espl

2008). Especially the brittle fracture zones substantially contributed to deep seated rock mass weakening and slope collapse, with fold structures and fracture sets providing preferred sliding planes (see Figure 2). For a detailed account of source rock units, structural setting, and valley-fill sediments, please refer to the accompanying online Supporting Information.

Deposit age and size

All dating data (obtained from three independent dating methods applied to different samples from different locations; Table I) coincide well and date the Tschirgant event into the middle Holocene at approximately 3 ka (Ostermann and Prager, 2014; Ostermann *et al.*, submitted: ESP-15-0234). Stratigraphic field differentiation of two individual accumulation events, as suggested by the dates in Patzelt (2012), however, is not evident (Patzelt, 2012; this study).

Estimates of the total volume of the accumulated debris are of the order $180–240 \times 10^6$ m^3 (Abele, 1974) and $200–250 \times 10^6$ m^3 (Patzelt, 2012), whereas reconstruction of the pre-failure Tschirgant ridge yielded 160×10^6 m^3 for the scarp niche (Pagliarini, 2008). This difference in volume between scarp and deposit can easily be explained by ~25% bulking due to dynamic rock fragmentation and dilation (see e.g. Abele, 1974; Erismann and Abele, 2001; Hungr and Evans, 2004). Drop height from the topmost scarp edge at 2160 m a.s.l. to the valley floor is 1400 m with a minimum runout distance of 6.8 km, and an area of over 9.8 km^2 covered with rock avalanche debris (Patzelt, 2012).

Data and methods

Field mapping was conducted at a scale of 1:1000 using LiDAR-derived hillshade images with 1-m resolution, digital orthophotos with a resolution of 2 to 2.5 cm, a handheld Garmin global positioning system (GPS), and a Thompson altimeter. All data were implemented in ArcGIS for digital mapping and spatial analyses. LiDAR images (flights between 2006 and 2010), the topographic base map, and orthophotos (2009) were provided by the federal government of Tyrol (www.tiris.gv.at). Excellent exposures of the otherwise vegetated (predominantly fir forest with extensive ground cover, e.g. Mair, 1997) rock avalanche deposit exist along the Inn and Ötz Rivers, along road cuts, and temporarily in construction pits. These outcrops were examined in detail. Additionally, oblique aerial photographs were taken by quad-copter flight surveys to support mapping of inaccessible outcrops (or parts thereof) and to provide better overviews of larger exposures. In the forested areas, megablocks (MB; herein defined as surface clasts over 1 m in diameter) and superficial erosion sites were used for lithological mapping, and plants and soils provided additional clues to underlying materials (especially moisture-indicative plants). A few available drilling reports yield information on thickness and grain-size of the landslide deposits as well as on pre-landslide valley deposits (Patzelt and Poscher, 1993; Hartleitner, 1993; tiris borehole register). Morphological terms such as hummocks and ridges are used according to Dufresne and Davies (2009).

Tschirgant Rock Avalanche Deposit

Herein we present the detailed lithological, morphological, and structural field surveys as well as analyses of remote sensing data (orthocorrected images, laserscan hillshade images) of the Tschirgant rock avalanche deposit. In this new map (Figure 3), the most striking feature is the spatial arrangement of the main lithological units: the central part is made up of Wetterstein Fm (WS) which is rimmed by Raibl Group (RG) debris. Thus, the source arrangement of sub-vertical, ridge-parallel layers (Figure 2) translated into a radial deposition pattern (Figure 3), preserving stratigraphy. The contact between the central Wetterstein and the outer Raibl beds, where exposed, is gradual and initially at a low angle. There is no evidence that Raibl Group may underlie Wetterstein Fm beds in the thick central parts where drill core reports document up to 65 m thick rock avalanche debris in direct contact with fluvial deposits (Patzelt and Poscher, 1993; see Tiris borehole register). Hauptdolomit was transported to the lateral edges, and small volumes of Alpine Muschelkalk are locally found near the transition area ('contact') of Wetterstein and Raibl deposits

Table I. Ages for the Tschirgant rock avalanche event from different methods

^{14}C (different wood/charcoal fragments)	2900 ^{14}C BP (*c.* 1050 BC)	Patzelt and Poscher (1993)
^{234}U/^{230}Th post-depositional carbonate cements	3650 ± 350 years and 2800 ± 100 years	Ostermann and Sanders (2009); Sanders et al. (2010)s
^{14}C (different wood/charcoal fragments)	3650–3450 cal. BP and 3070–2950 cal. BP	Patzelt (2012); see also Prager et al. (2008)
^{36}Cl (boulder surface exposure)	2980 ± 500 years	Ostermann and Prager (2014); Ostermann *et al.* (submitted for publication)

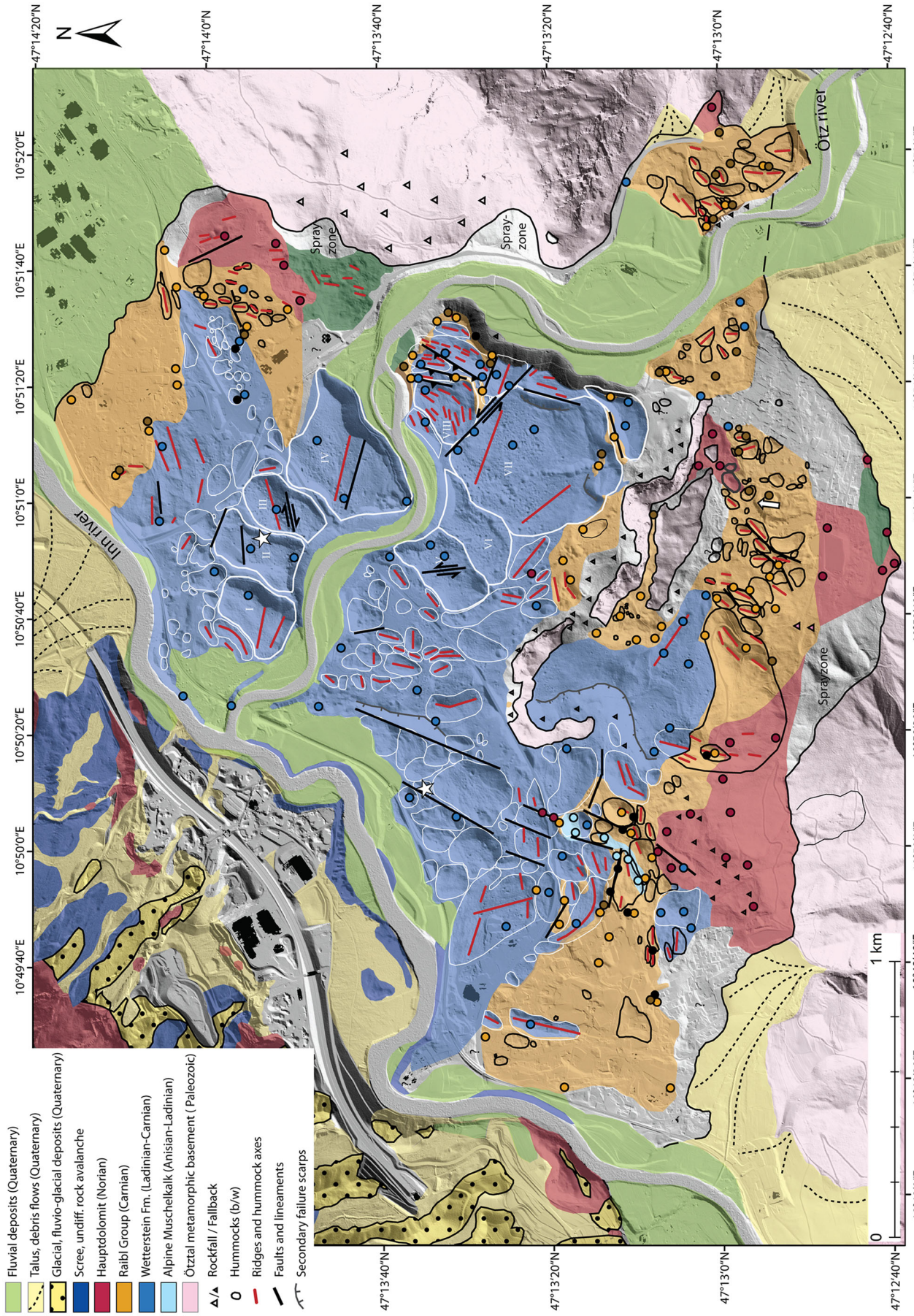

Figure 3. Geological, morphological, and structural map of the Tschirgant rock avalanche deposit. Thick white outlines and roman numerals mark the rockslide depositional area, whereas hummocks of the spread rock avalanche deposit are outlined by thin white and black lines. The white stars mark drill sites KB7 (west) and KB14 (east). This figure is available in colour online at wileyonlinelibrary.com/journal/espl

(e.g. Roppen; see Figure 3). At several locations, polymict gravels (dominated by metamorphic rock fragments, e.g. gneisses, amphibolites) are encountered atop the rockslide deposits, mingled therein or as a whole unit.

The majority of the Tschirgant deposit shows pristine rock avalanche morphology without significant erosional modification. River incision created extensive longitudinal and transverse sections through the entire deposit depth. Onlapping of alluvial fans is minor in the Sautens area, whereas rockfall activity at Amberg partially obscures runup and sprayzone deposition. Modification of the largest part, however, is insignificant.

Beyond the proximal accumulation area the emplacement of the Tschirgant rock avalanche deposit was significantly influenced by the NW-SE-oriented Rammelstein bedrock ridge situated at the mouth of the Ötz valley. It divided the deposit into two areas; herein simply referred to as the northern and the southern area. All major features mentioned in the text are summarized in Figure 4.

Proximal areas

Before the Tschirgant rock avalanche was split into two lobes by the Rammelstein bedrock ridge, it crossed the Inn River and deposited up to at least 65 m thickness (Patzelt and Poscher, 1993: borehole KB7, see also Figure 3) of Wetterstein carbonates. Three features are prominent in this roughly 500 m wide and 1500 m long proximal stretch (Figure 4). One is a long ridge in northward (i.e. proximal) extension of Rammelstein. It is unclear if the *in situ* bedrock extends beneath this rock avalanche ridge, but it is a likely explanation for this morphological feature. The other outstanding feature is a 400 m long and 35–40 m high cliff adjacent to the aforementioned ridge (Figure 4). At its foot, the rock avalanche morphology looks like fallback (a secondary feature where avalanche debris falls back onto itself after partially travelling up a steep slope; e.g. at the distal Socompa volcanic debris avalanche; Kelfoun *et al.*, 2008), i.e. Brandung (after Heim, 1932). The cliff's NNE orientation is paralleled 240 m to the west by a less conspicuous lineament between hummocks; possibly the other side of the pre-avalanche Inn River. Further lineaments exist in line with the large cliff and to the SW at the base of Holzberg slope. The third feature consists of several larger, flat areas (ruled signature in Figure 4).

Northern area

Rockslide

The northern area is dominated by very large (up to 550 m diameter) hummocks (I–VIII in Figure 3) in its central part. Their very large sizes, long axes orientations transverse to sliding direction, and their jigsaw-fit arrangement strikingly resemble rockslide deposits (e.g. Hancox and Perrin, 1994; Dufresne *et al.*, 2010). In addition, each hummock (or group of hummocks) shows individual characteristics. Hummocks I–IV have rectangular shapes and are separated by morphological gaps (graben structures) tens of metres wide and deep. Hummocks III, IV, and VII furthermore contain longitudinal ridges paralleled by lineaments ('faults') striking at 077°, 097°, and 110°/140°, respectively. The last values correspond to the approximated failure trajectory towards SSE; whereas 077° shows the onset of lateral spreading down the broad Inn valley.

On the true left side of the Ötz River, hummocks V–VIII lie in direct contact to each other. Here, lateral spreading was restricted by the Rammelstein bedrock ridge. Up until hummock VIII, a carapace with an open network of megablocks 10^0–10^1 m in size exists. From here to Amberg, the disappearance of the carapace is accompanied by a change in morphology marked by rising topography, ridges oriented perpendicular to sliding direction, and faults, plus an interior dominated by highly crushed material. A fortuitously large and unvegetated cliff exposes 150 m of this zone down to the basal rock avalanche contact at about 30 m below the terrain line (Figure 5). The hummock at this transition (VIII) is surrounded by unusually deep and narrow valleys (Figure 6A). In the valley between hummocks VII and VIII exists a small (~2 m high) mound

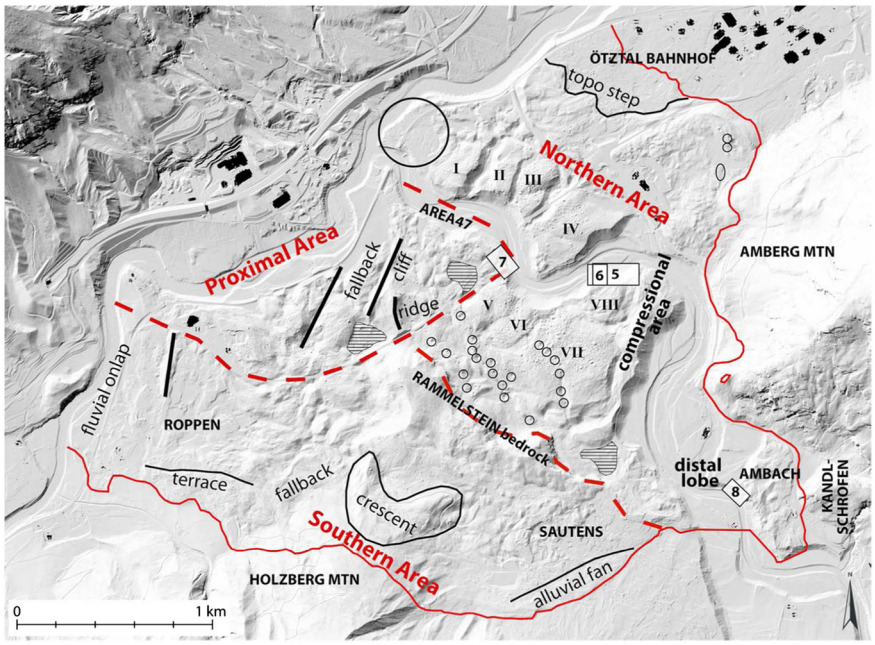

Figure 4. Map showing the locations of the major features discussed in the text. Outcrop locations of Figures 5–8 are marked by white boxes with the respective figure number shown. Red dashed line marks the 'boundaries' between the three depositional areas (proximal, northern, and southern). Large circle: area with small circular depressions; small circles: locations of some larger circular depressions; hatched signature: flat areas. LiDAR hillshade image from tiris (https://portal.tirol.gv.at). This figure is available in colour online at wileyonlinelibrary.com/journal/espl

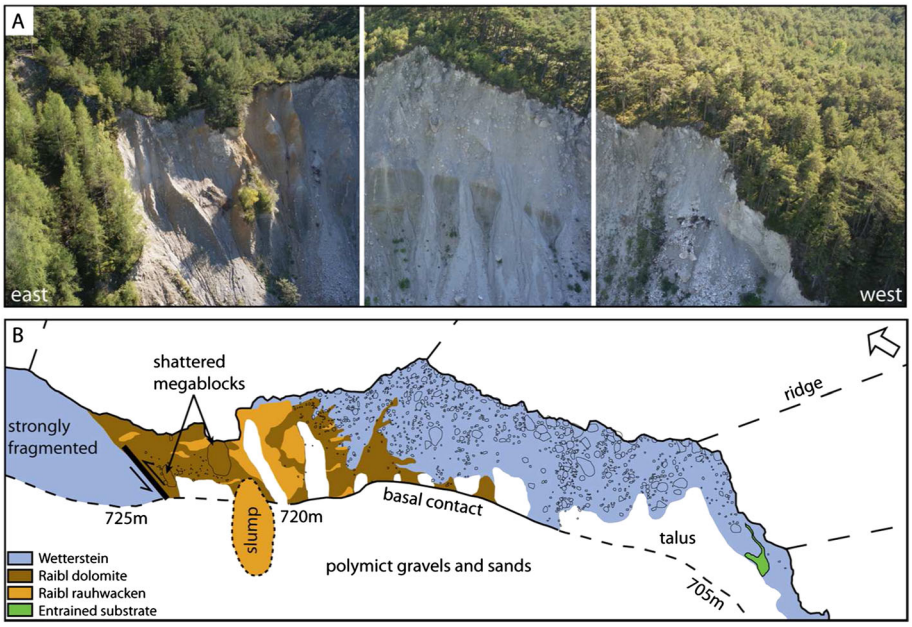

Figure 5. Rockslide hummock VIII (to the right of Raibl and fault) and transition to the collisional zone (left of Raibl) with distinctly more fragmented rock avalanche material, phantom blocks, and diminished megablock cover. This figure is available in colour online at wileyonlinelibrary.com/journal/espl

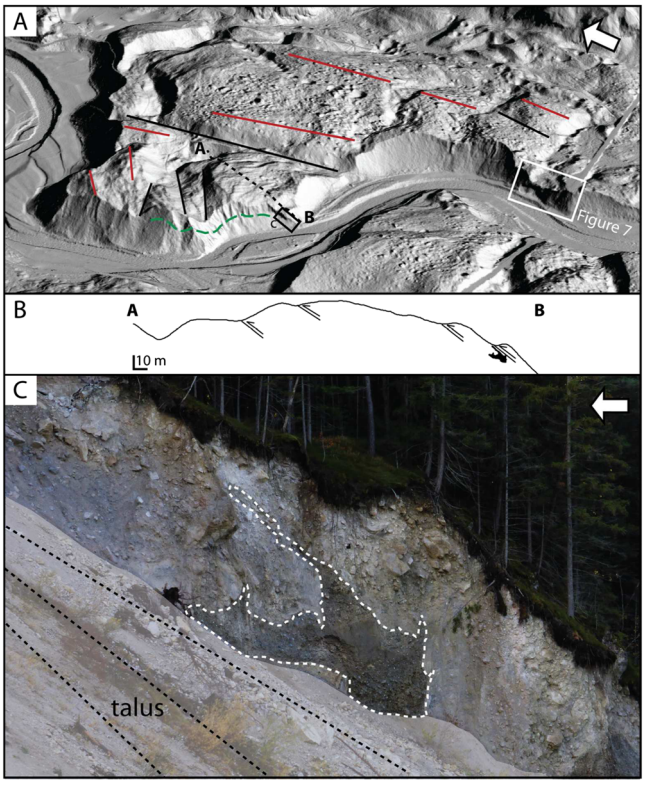

Figure 6. (A) LiDAR hillshade image (oblique view to south, i.e. rock avalanche propagation, (B) of the medial rockslide deposition: dashed green line shows basal contact. (C) Dashed outline around injected/intruded polymict gravels and sands (rock avalanche propagation from right (NW) to left (SE). This figure is available in colour online at wileyonlinelibrary.com/journal/espl

composed of a mixture of angular rockslide clasts and rounded, unbroken polymict gravels.

In this northern accumulation area, several interesting, correlated features are observed. Firstly, the shape of the terrain line follows that of the basal rock avalanche contact (Figure 5). Secondly, surface ridges change orientation from slightly oblique to perpendicular to sliding direction. Thirdly, debris of the Wetterstein Fm transits into and overlies those of the Raibl Group. The three features in detail:

1. The material underlying the rockslide deposit in sharp contact consists of disrupted, polymict coarse sands devoid of original depositional structures. Downwards, the sands transit into fluvial gravel-and-sand mixtures. At the distal end of this large exposure, polymict, gneiss-boulder-dominated gravels again form a concave contact, and again the terrain line of the rock avalanche runs parallel to this contact shape (dashed line in Figure 6A).
2. At the most proximal exposure end, the ridges are only slightly oblique to sliding direction (Figure 5B). Where the deposit surface steadily increases in height and megablocks disappear, these ridges swing into a motion-perpendicular orientation.
3. The contact between Wetterstein carbonates and Raibl debris is initially at a low angle of apparently 10°–30° (dipping roughly towards the northwest; Figure 5), with some intercalations of the two lithologies and a steeper contact towards the east. Raibl rauhwacken are included as a wedge, and down-motion of this wedge they are found sheared in banded succession with (Raibl) dolomites; the bands run roughly parallel to the deposit surface.

An important detail for rockslide and rock avalanche motion and internal deformation is exposed at the most proximal exposure end (Figure 6C). At this (and other locations, e.g. near the federal road bridge at Area47, and at the distal location Ambach), entrained valley-fill sediments are surrounded or bordered by distinctly more fine-grained rock avalanche material (Figure 6C). Their presence and deformation highlights rock avalanche processes otherwise not readily visible in this monochromatic part of the deposit.

Between the rockslide and Rammelstein ridge is a 30–200 m wide accumulation area of predominantly Raibl rauhwacken. Apart from one large hummock in oblique contact with the bedrock ridge, the rauhwacken occurrence is restricted to the lower topographic regions and to the lowest slopes of Wetterstein hummocks. Extrapolating the geometric

relationship between Wetterstein and Raibl beds from the previous locale to here, a low-angled approximately N-facing contact with Wetterstein overriding Raibl debris seems reasonable.

The proximal transition from scattered hummocks (rockslide 'wake') to hummock V of the rockslide is marked by a topographic low occupied by fluvial sands and gravels (Figures 4 and 7). This site has previously been mentioned by several authors (Ampferer, 1904; Patzelt and Poscher, 1993; Abele, 1997; Erismann and Abele, 2001; Prager *et al.*, 2012; Patzelt, 2012), but has hitherto not been studied in detail. It shows the following features:

- Lack of stratification in the fluvial deposits (Figure 7C);
- Imbricated rock avalanche fabric (Figure 7A), i.e. blocks are aligned and dip in travel direction, as well as fractures through the blocks oriented perpendicular to travel direction (Figure 7B);
- Pebbles of the intruded polymict gravels and sands are aligned parallel (long axes) to the sediment-rock avalanche contacts;
- Upward-fining sands intruded all the way up to the terrain line and there are signs of rock avalanche disruption by the intrusion as well as dewatering structures ('Pavoni pipes', Pavoni, 1968; Figure 7C).

Circular depressions

Among the many intricate morphological details revealed by the LiDAR images (see Figure 4) are two sets of circular depressions. One set is located at the Inn–Ötz confluence; here most of the scattered holes are 5–7 m in diameter with only a few reaching a maximum of 10 m with depths between 0.5 and 2 m. Indlekofer (2014) summarized documentation of World War II bombardments aimed at destroying the railway bridge (e.g. Unterrichter, 1949; Albrich and Gisinger, 1992; Mahoney, 2013), as well as bomb findings during recent railway construction (Richter, 2010), underlining human conflict as their cause. However, the other set of circular depressions lies along rockslide hummocks VI–VII (see Figure 4) and in the band between rockslide and Rammelstein ridge, and therefore outside the documented bombing site. Furthermore, the features here are larger, up to *c.* 20–30 m diameters and 3–10 m depth. They are preferentially arranged along NNW to WNW trending lineaments instead of scattered randomly. Circular to funnel-shaped depressions are also encountered at other Holocene rock avalanche deposits, e.g. the nearby carbonate Fernpass sturzstrom (Abele, 1974; Prager *et al.*, 2006, 2009); however, it remains unclear whether these features originate from syn- and/or post-kinematic processes. With respect to the lithological units encountered in the Tschirgant area (fractured carbonates, Raibl rauhwacken), here these depressions may be attributed to karst and sinkhole processes, e.g.:

1. Several rock units of the Tschirgant massif have carbonate karst potential, especially the thick limestones and dolomites of the Wetterstein Fm. Besides carbonate karst, in the Tschirgant area sulphate karst phenomena are likely to be encountered, since the Raibl rauhwacken can contain gypsum and thus cause distinctive sulphate mineralization of the groundwater (e.g. spring Römerbad at the Tschirgant slope toe; compare Weber, 1997; Probst *et al.*, 2003). Sinkholes are present in some nearby areas made up by Raibl beds (Goldberger, 1947, 1950).
2. At Tschirgant, the Wetterstein carbonates locally overly the Raibl beds at a low angle (Figure 5). Since the fine clastic Raibl beds pose impermeable layers (aquiclude/aquitard), these can locally pond groundwater in the overlying fracture and karst aquifers, and thus cause subrosion/suffusion in the saturated carbonate units.
3. Another explanation may be related to syn-/post-emplacement dewatering of the saturated substrate (i.e. alluvial valley sediments, affected by undrained loading during rock avalanche emplacement). A partially subterranean channel, and sinkholes in linear alignment with this channel, in the north-eastern deposit part (Figure 4; near contact to Amberg Mtn; see later) are further indications for subrosion and suffusion processes, respectively.

Collision (Amberg)

The rock avalanche morphology parallel and to the north of the rockslide, near the mountains of Amberg Mtn, is strongly lithology-controlled. The largest, elongated hummocks are formed by Wetterstein Fm (Figures 3 and 4). Immediately

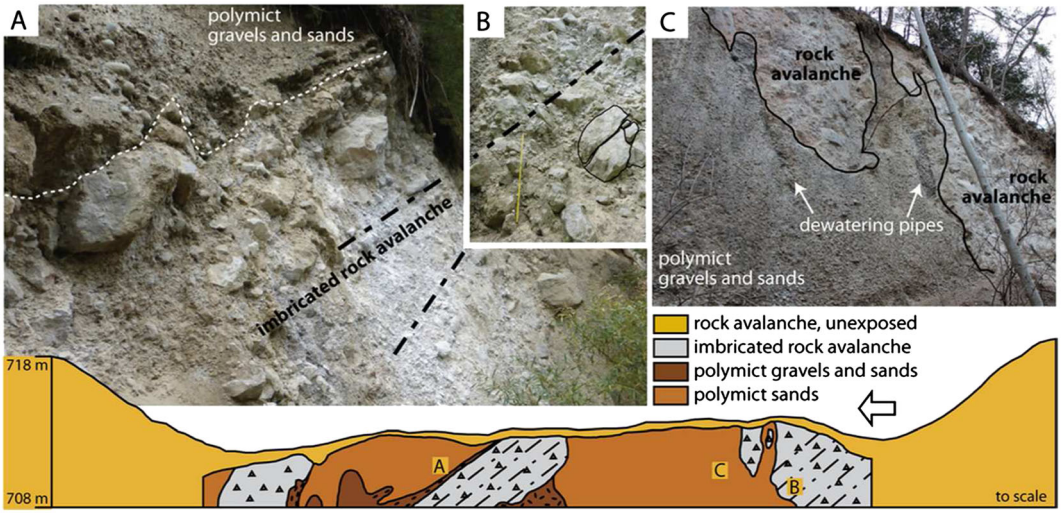

Figure 7. Outcrop at the true left bank of the Ötz River, near the federal road bridge, Area47. In a topographic low point between two hummocks, fluvial gravels and sands are injected all the way through the rock avalanche cover. Their pathways follow rock avalanche fabric (A), but also cut through and disrupt it (C). Fractures in rock avalanche clasts are parallel to imbricated RA fabric (B); grey signature in sketch), respectively perpendicular to travel direction (white arrow). Pebbles in the intruded coarser polymict gravels and sands (dark brown signature in sketch) are aligned parallel to sediment-rock avalanche contact. Upward-fining sands (light brown signature in sketch) intruded vertically all the way to the top of the exposure, with signs of rock avalanche disruption and de-watering pipes (C). This figure is available in colour online at wileyonlinelibrary.com/journal/espl

down-motion, Raibl debris forms a band of smaller hummocks. The distal rim facing down the Inn valley is raised and comprised of Hauptdolomit. Closer to the centre of this area, Hauptdolomit boulders are consistently of the order of maximum 0.5 m in diameter; and they are also found higher on the slopes of Amberg as scattered, single rock avalanche boulders. The distinct morphological pattern (dark green signature in Figure 3) seen on the LiDAR hillshade image is due to an area characterized by gneiss boulders (i.e. 'block-sand terrace' attributed to late-glacial flood-sheets, Heuberger, 1966, 1975; see also map by Patzelt, 2012). Most hummock long-axes in this whole area are oriented perpendicular to the local rock avalanche motion directions.

Lateral spreading (down-valley; Ötztal Bahnhof)

Concurrent with disappearance of megablocks is an abrupt change to a ~25 m lower topography and longitudinal ridges in the northern lateral area (Figure 4). Here, the debris was able to spread unhindered down the 2–2.5 km wide Inn valley. Also, a lithological change to mechanically weaker and highly sheared Raibl beds begins here. Unlike the source area geometry, where ochre Raibl rauhwacken and grey-brown dolomites occur as distinct beds, in the rockslide–rock avalanche deposit these two lithological units are sheared into long, thin bands (compare to Figure 5).

Distal deposition (Ambach), compound hummocks, and basal mixed zone

The distal lobe is situated between Rammelstein ridge to the west and Amberg/Kandlschrofen to the east (Figure 4). It is composed of Raibl beds, with only few Wetterstein megablocks on top of hummocks on the true left side of the Ötz River, and some 0.1–0.5 m sized Hauptdolomit boulders in a runup zone at a sub-vertical bedrock cliff on the other side (Kandlschrofen; see Patzelt, 2012).

Even at this distal location, the original stratification of the source rock bedding is preserved. The relative height of hummocks varies between less than 5 m and more than 20 m. In general, hummocks below 10 m tend to be more conically shaped, whereas the higher structures appear less clear and at times form elongate ridges with a narrow base. Compound hummocks [several hummocks merged into one feature (Clavero *et al.*, 2002); see also Figure 13D later] are predominantly aligned in a NE-SW direction, i.e. perpendicular to the rock avalanche travel direction, swinging to NNE-WSW with distance. Figure 8 shows the north-western end of a 25 m long

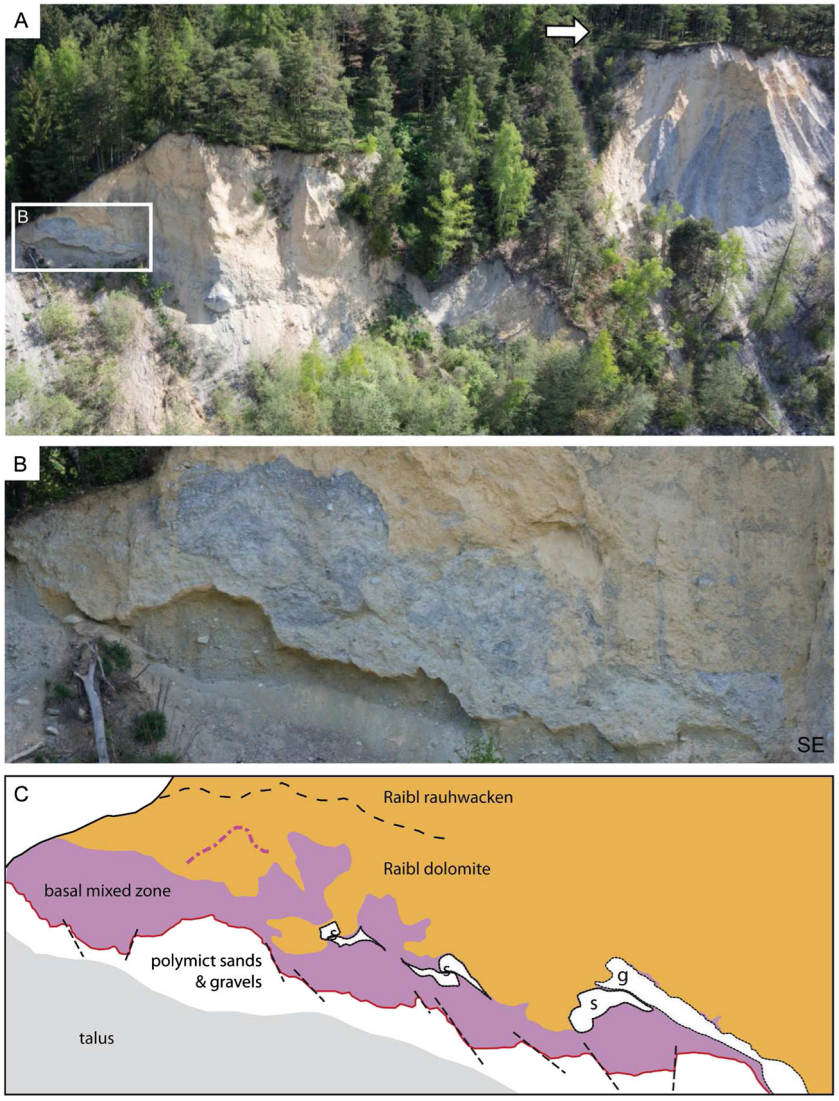

Figure 8. The distal rock avalanche, Ambach, orographic right side of the Ötz River: (A) two compound hummocks with basal contacts indicated (see also Figure 10); (B) close-up of the most accessible basal contact and its interpretation; (C) highlighting a basal mixed zone, small normal faults and graben structures at the basal contact, rip-up sandy clasts 's' and substrate injections ('g', gravels and sands). White arrow shows motion direction. This figure is available in colour online at wileyonlinelibrary.com/journal/espl

section of a cut approximately right-angled through a transverse hummock, and a thick layer of thoroughly fragmented Raibl rauhwacken overlying (Raibl) dolomite debris and a thin, 1–2 m basal mixed zone. The different layers of debris dip with direction of the rock avalanche towards the southeast. *In situ* sediments are graded and stratified, but disrupted by several steep faults with offsets between 0.4–1 m (Figure 8C). Within the basal mixed zone, different mobilized sediments are either mixed into rock avalanche debris or are entrained as rip-up clasts or along narrow faults that also dip in flow direction (Bösmeier, 2014).

Southern area

Lateral deposition (up-valley; Roppen) and Runup (Holzberg)

The area of Roppen village is extensively settled, but it appears that anthropogenic modification was focused on morphologically flatter and less rugged areas since the actual settlements end at steeper topographies. Plus, remnants of gentle hummocks and river terraces are discernible on the LiDAR images, ascertaining that the original rock avalanche topography has not been modified beyond recognition. One long Wetterstein ridge stands 10 m above the surface to the southeast and 20 m above the riverside topography to the northwest (Figures 3 and 4). Its long axis strikes at 190°, which fits with expected spreading direction at this locale (furthermore, megablocks on the crest have matching bedding orientations around 190/25 and 210/40). Fluvial on-lap west of this ridge created a flat, terraced morphology (Ampferer, 1904: approximately 15–20 m thick gravely-sandy backwater terraces).

The entire Roppen area is dominated by Raibl debris. Their distribution is evident in many construction pits (open at the time of mapping), residents' reports of older excavations, and in low-lying topography. Larger hummocks of (Wetterstein Fm) carbonates become increasingly more separated from each other with distance. In the depressions between them, and at the source-ward slopes of Wetterstein Fm hummocks that are not separated, are small occurrences of Raibl rauhwacken (Figure 9). After a few isolated Wetterstein Fm hummocks, Raibl Group beds take over and form more subtle and flatter deposit morphology with overall relatively small hummocks. A larger, steep hummock with megablocks of cemented breccia is situated towards the distal margin. Such megablocks also exist at the transition from Wetterstein Fm to Raibl Group 400 m to the NE, right at the Wetterstein Fm–Raibl Group transition, and they might have been calcified slope talus and/or paleoreef breccias (see Prager, 2010) transported to this locale as part of the rock avalanche.

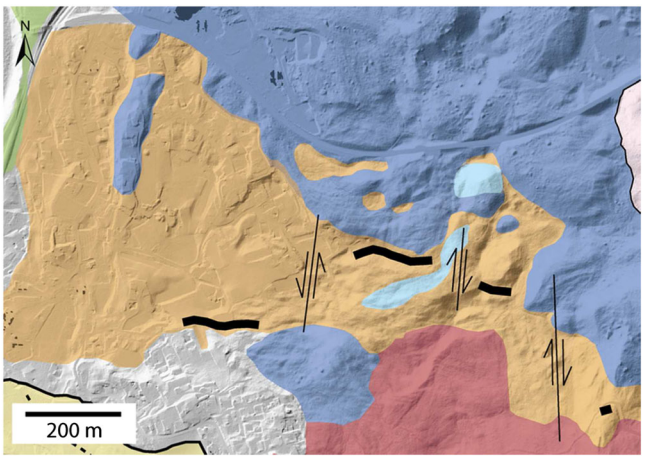

Figure 9. Raibl clayshale (thick black lines) offset in the Mairhof-Roppen area might indicate incipient debris lobe formation along the inferred lineaments ('faults'). For legend please refer to Figure 3. This figure is available in colour online at wileyonlinelibrary.com/journal/espl

Naturally exposed 'bands' of Raibl clayshales (Figure 9) striking WNW-ESE (110°), with partially only minor rock fragmentation (i.e. still featuring decimetre-sized, densely bedded/schistose clayshale blocks) are offset to each other along inferred lines that coincide with spreading direction (190°). The clayshales reappear high up on Holzberg ridge (bottom right corner of Figure 9).

Pre-existing fluvial terraces can still be seen through the deposit on LiDAR images. Edge-rounded limestone clasts are scattered on top of these terraces. Runup at Holzberg northern slope reached 920 m a.s.l., and is, as a mirror image of the northern deposit area, composed of Hauptdolomit (Figure 3). Fallback has created rockfall fans (Figure 4) of Hauptdolomit boulders of which most are less than about 0.5 m in diameter (few reach roughly 2 m).

Bedrock ridge overtopping (Rammelstein) and distal deposition (Sautens)

The most peculiar rock avalanche hummock of Tschirgant is situated on the NNE slope of Holzberg (Figures 3 and 4). It is crescent-moon shaped and nestled up against the slope to a height of 888 m a.s.l. It thereby sits roughly 100–125 m above the northward-bounding deposit surface and 70 m above the down-motion surface. From north to east along the NNE trending high ridge (left 'leg') of this hummock, lithology transits from Wetterstein with characteristic megablocks to (Raibl) dolomites, clayshales, again dolomites, and eventually rauhwacken. The clayshales are broken into small fragments that are rotated relative to one another. In a large outcrop of ochre rauhwacken (roadcut Sautens-Roppen at 860 m a.s.l.; Figure 4) remains nothing but once clastic material sheared to silt and clay sizes ('fault gauges'); with only the odd < 15 cm survivor clast and the occasional nest of crushed dolomite. The latter then forms its own facies towards the north of the exposure. Following the crescent down-motion, ridge orientation changes to N-NNW until a *c.* 10 m deep incision marks a break in morphology on this other 'leg' of the crescent. Here, a high northward flank and a steep southward cliff riddle the possibility of very sudden stopping, cliff collapse, and further spreading of the collapsed mass. Parallel to the Raibl crescent, Wetterstein debris overtopped Rammelstein ridge and moved into the valley behind, first depositing as large half-round hills on the ridge crest, then as one longitudinal ridge. The latter sits on top, respectively is surrounded by a rim of Raibl rauhwacken, which form smaller hummocks. Arcuate compressional lines are visible in the deposit morphology down-motion (Figure 4) and might be related to flow into a shallow lake. An entrained clast of lake sediments was exposed (until late 2013) in a subsequently filled commercial pit in Sautens village just behind the arcuate ridges.

The lateral-distal deposition is again formed by a small patch of Hauptdolomit. Further on, the deposit surface is completely obscured by Sautens village. Markedly though, the topography of the 'old' (pre-rock avalanche) alluvial fan is still visible through the rock avalanche deposit surface on LiDAR images, and it is here that we find a small rim of bulldozed gravels and sands (dark green signature in Figure 3).

Megablocks

The highest density distribution of megablocks is on the rockslide part (hummocks I–VIII) of the deposit (Figure 10). Here, 59% of the 2230 megablocks mapped are located on roughly 0.6 km^2. This amounts to 22 megablocks per 10^4 m^2,

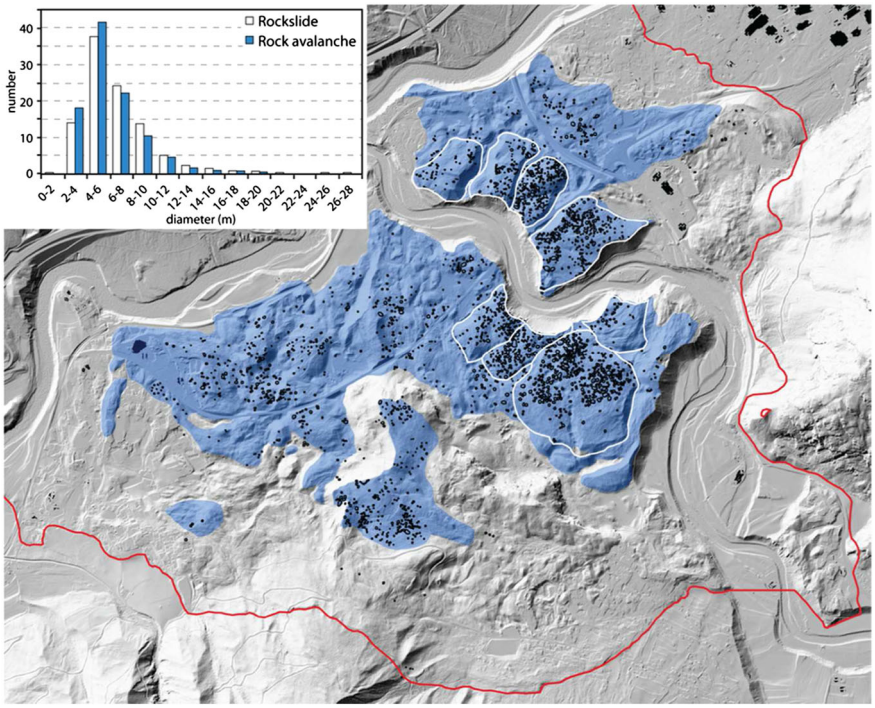

Figure 10. Megablock density distribution map: the Wetterstein map signature is adjusted to show only the surface of deposition. The highest density distribution of megablocks (black outlines) is on top of the rockslide are (hummocks outlined in white). Their relative size distribution (inset), however, is equal in both the rockslide and the rock avalanche areas. This figure is available in colour online at wileyonlinelibrary.com/journal/espl

whereas the remaining rock avalanche part of the Wetterstein depositional area only has five. The inset of Figure 10 shows the size distributions of megablocks on top of the rockslide and rock avalanche areas, respectively.

Emplacement velocity

A measured 920 m a.s.l. runup rim at Holzberg and an estimated crest elevation (before rock avalanche cover) of 830 m a.s.l. for Rammelstein Ridge, together with an estimated original Inn valley level at roughly 700 m a.s.l. (from basal contacts in drill cores at KB14 and allowing for some valley-fill erosion by the rock avalanche) are the basis for velocity estimates. Using the equation $v = (2 \times g \times h)^{1/2}$ results in theoretical maximum velocities of 51 and 66 m/s (184 and 238 km/h), which is well within the range recorded, calculated or estimated for other rock avalanches [e.g. 30–360 km/h, Erismann and Abele, 2001; Hungr and Evans, 2004; further case-studies and references in Prager (2010)]. Assuming an average of 160 km/h for the runout path gives an approximate runout duration of the order of two to three minutes. In comparison with recorded historical events (Weichert *et al.*, 1994; Ekström and Stark, 2013) these numbers appear reasonable.

Discussion

Differentiating between deposits of different genesis requires correct understanding of the processes leading to the formation of a particular landform (e.g. Hewitt, 1999). Previous studies have already indicated that at Tschirgant the morphological features reflect emplacement dynamics (e.g. Abele, 1997; Erismann and Abele, 2001; Patzelt, 2012; Prager *et al.*, 2012; Dufresne *et al.*, 2014). Herein we discuss the factors and processes we deem most critical in shaping rock avalanche deposits in an order of perceived ascending importance.

Substrate interactions

The role of runout path materials in the emplacement of rock avalanches has evolved over the past decades. At times they were proposed to be the most important factor in explaining the excess runout of large, catastrophic rock avalanches either through undrained loading or by causing transformation into debris flows (Hutchinson and Bhandari, 1971; Legros, 2002; Hungr and Evans, 2004; van Asch *et al.*, 2015). Elsewhere they were assigned an accessory role for the description of basal deformation features; entrainment, injection, and mixing was noted but not elaborated further. Through the years, many researchers recognized their potential to shape rock avalanche deposits (Abele, 1974, 1997; Hewitt, 1988; Erismann and Abele, 2001; Hungr and Evans, 2004; Prager *et al.*, 2008, 2012; Dufresne, 2009; von Poschinger and Kippel, 2009; Dufresne *et al.*, 2009, 2014). At Tschirgant, we found evidence of the direct involvement of substrates in shaping rock avalanche morphology. We furthermore emphasize their importance in (highlighting) internal avalanche processes. Indications for significant runout alterations through substrate interaction are not evident for the Tschirgant rock avalanche, but have been observed elsewhere (see summary in Dufresne *et al.*, 2009).

Substrates can actively shape the final morphology of a rock avalanche. The long exposure near the gravel bar in the Ötz River (Figure 5) superbly shows how rock avalanche debris, while overriding stationary, deformable substrates, can push them into a wave-like form so that its own surface geometry corresponds to the contact shape of these two units (Figures 11A, 12C and 12D). Field observations at the Ollagüe volcanic debris avalanche in Chile (Clavero *et al.*, 2004) and the Fernpass rock avalanche in the European Alps (Prager *et al.*, 2006, 2009), as well as analogue experiments (Dufresne, 2012) illustrate how decelerating upper material can be passively transported a further distance on top of a still mobile, lower unit. The final landform must hence be linked to the processes within this lower unit.

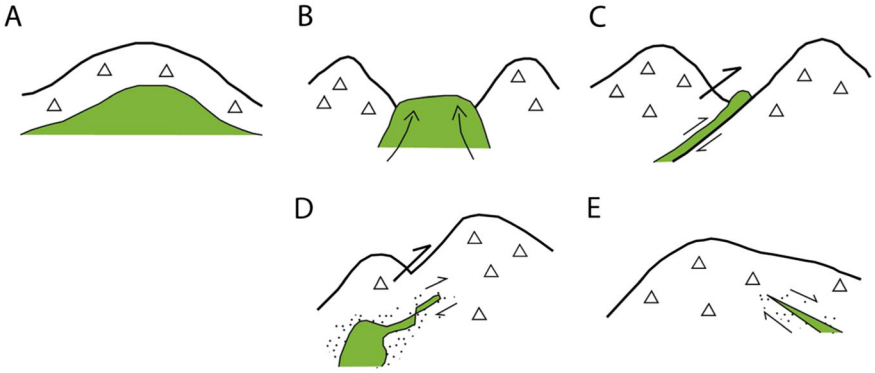

Figure 11. Sedimentary runout path materials (green) actively influencing rock avalanche morphology: A, bulldozed sands beneath the rock avalanche give the rock avalanche terrain line its shape; B, where extension between two hummocks allowed saturated sands and gravels to rise to the surface, they form the rock avalanche terrain in this area. The other sketches show how substrates act to highlight faulting and other emplacement processes: C, small gravel-sand hummock created by transport of substrate material along a fault; D, shearing and offset along internal planes of rock avalanche motion; E, injection of substrate material along normal fault that is created during very late deceleration stages. Stippled signatures mark areas of very fine grained rock avalanche material interpreted as shear zones. This figure is available in colour online at wileyonlinelibrary.com/journal/espl

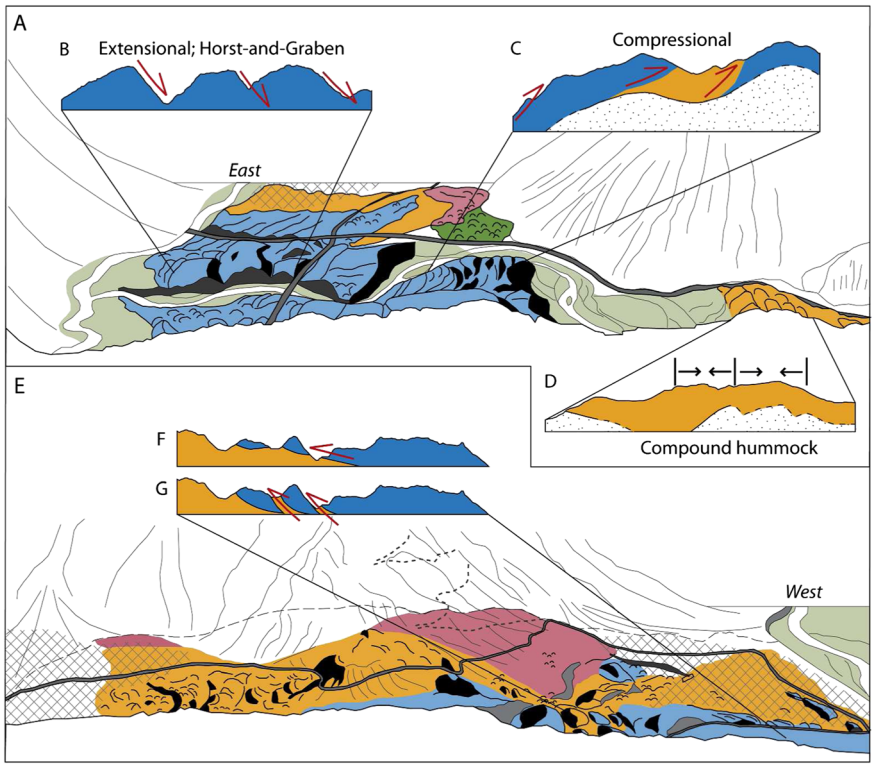

Figure 12. Summary sketch of the some of the main features of the Tschirgant rock avalanche deposit (for legend please see Figure 3; hatched areas are settlements). A, The rockslide and avalanche north of Rammelstein bedrock ridge; B, large rockslide hummocks in cross-section with potential formation style indicated; C, overriding of fluvial sands and gravels. This sketch shows how the rock avalanche surface mimics the shape of the disrupted substrates. Furthermore, thrust faults and insertion of Raibl rauhwacken between Wetterstein hummocks are carved out. D, Deposition on deformable substrates and compound hummock formation at the distal deposit; E, the rock avalanche to the south of Rammelstein bedrock ridge; F and G, two possible configurations of Raibl and Wetterstein in Roppen town (F indicates spreading in extensional regime, whereas G the more likely scenario of compression akin to C). This figure is available in colour online at wileyonlinelibrary.com/journal/espl

Phenomena related to substrate bulldozing are commonly known for deposit margins, e.g. Shiveluch volcanic debris avalanche (Belusov *et al.*, 1999). So also here at Tschirgant: small rim at the transition to a large alluvial fan in Sautens and locally in the northern area (dark green signatures in Figure 3). Isolated flat areas within the deposit are also inferred to be related to local substrate interactions. Dufresne *et al.* (2009) observed such flat areas in association with bulldozed substrate materials and situated immediately before a next, large rock avalanche hummock or ridge; in a sense a 'topographic' obstacle.

Evidence of extension and compression (see later) between rock avalanche hummocks is highlighted by substrate entrainment. Figure 11B (please compare to Figure 7) depicts the end-result of two possible scenarios. In one interpretation, the rock avalanche formed hummocks in horst-and-graben style (Figure 12B), i.e. by extension (similar to the nearby Fernpass rock avalanche; see Abele, 1997; Prager *et al.*, 2006, 2009). Into this region of extension and thus lessened overburden pressure, the loaded, saturated fluvial sediments penetrated through to the rock avalanche surface. Another possibility is inferred from the rock avalanche fabric. From studies of pyroclastic flow deposition, researchers have shown that imbrications result from gradual deposition rather than from mass freezing (e.g. Kamata and Mimura, 1983). At this locale behind the rockslide, rock avalanche material arrived on saturated valley-fill material already disrupted by the passage of the

rockslide; and so they might have gradually deposited onto or into the disrupted sediments. Faced with an area of lesser overburden, the sediments then escaped upwards, just as in the extension scenario (Figure 11B). Some substrate moved along the rock avalanche imbrication lines, while other volumes went straight upwards, creating their own pathways and disrupting rock avalanche features. Both scenarios are plausible, and a combination of the two is likely. Evidence for water-saturation of the fluvial sands and gravels at the time of disruption includes upward-fining of the substrates, imbrication of substrate clasts, and dewatering pipes (Pavoni, 1968; see also Patzelt and Poscher, 1993; Abele, 1997; Prager *et al.*, 2012).

The occurrence of individual mounds made of rounded, uncrushed substrate clasts or a mixture of intact substrate and broken rock avalanche clasts between hummocks or along linear depressions may indicate the locations of faults in the rock avalanche debris that are directly related to rock avalanche emplacement (Figure 11C). These inferred faults are akin to internal deformation seen in analogue experiments by Shea and van Wyk de Vries (2008) and agree with field observations elsewhere. Diapirism similar to Figure 11B, but along narrower pathways, supplies an alternative (or concurrent) mechanism for these mixed mounds.

The next two sketches in Figure 11 depict two examples of substrates as visual markers which highlight the end-products of short-lived emplacement processes. Substrates picked up at a hummock front, respectively entrained along a fault, are sheared along the contact upon collision with the next hummock, and the sheared 'tongue' is subsequently offset during deformation when the two hummocks collide (Figure 11D; please compare to Figure 5); a deformation that was already inferred from morphometric analyses prior to cross-section analysis. Figure 11E shows a distal normal fault which we interpret as the result of gradual deposition of hummocks under extension (rock avalanche motion from left to right) of the decelerating rock avalanche front. In both cases, the entrained substrates are surrounded by a 'halo' of very fine rock avalanche material. This we interpret as shear zones, which provide favoured pathways for substrates to penetrate into the moving mass along these zones of weakness or even temporary openings in the granular network.

Topographic interference

Runout path topography induces considerable complexities in the final deposit shape and morphology of rock avalanches (e.g. Nicoletti and Sorriso-Valvo, 1991; Erismann and Abele, 2001). Hewitt *et al.* (2008 p.11) summarized an important observation made throughout the landslide literature: 'because rock avalanches have great kinetic energy but lack cohesion and tensile strength, topography can concentrate, disperse, or split the debris stream horizontally and vertically (Heim 1932; Abele 1974; Fort 1996; von Poschinger 2002)'. In fact, it is rare to find rock avalanches that did not encounter any smaller or larger topographic obstacle in their paths (<5% unobstructed runouts in a set of 178 worldwide deposits; Dufresne, unpublished database). Hewitt (2002) reports nothing but evidence for persistent rock avalanche-topography interactions and resulting complex deposit morphology from the vast number of rock avalanche deposits in the Karakoram Himalayas. Likewise, the emplacement topographies in the European Alps are relatively confined.

At Tschirgant, splitting of the streaming debris by the Rammelstein bedrock ridge significantly affected neither the preservation of source stratigraphy nor of motion indicators. The differences in interactions with topography on either side of the bedrock ridge reflect the interrelation of lithology and processes, together with terrain conditions and emplacement regimes. For example:

- Compressional ridges from frontal collision with the mountains of Amberg Mtn (northern area; Figure 12C);
- Transform fault between collided debris and those masses still moving up the Ötz valley (Figure 6A);
- Runup and fallback at Holzberg Mtn (southern area);
- Crescent-shaped deposit of caroming lateral flow along the side of the Holzberg Mountain;
- Bedrock ridge overtopping and streaming ridges down into Sautens area with again typical longitudinal ridge indicating motion direction.

Resistance to lateral motion at the distal end caused sinistral shearing and subsequent oblique long-axes orientations of hummocks (Bösmeier, 2014). They are assumed to represent transverse ridges associated with deceleration and compression of the debris mass (Dufresne and Davies, 2009) presumably due to the ascending topography into the Ötz valley and interaction with existing valley fill sediments (Figures 8 and 11E). This local retardation also explains the formation of compound hummocks (Figure 12D).

Furthermore, overtopped river terraces are still visible (on LiDAR images) through the rock avalanche deposit, a phenomenon generally only known well for thinner (a few metres in thickness) rock avalanche deposits, particularly those emplaced over glacial ice (e.g. Sherman Glacier, McSaveney, 1978; Black Rapids Glacier, Jibson *et al.*, 2006; Acheron, New Zealand, Smith *et al.*, 2006). Yet, even the thicker Tschirgant deposit shows evidence of fluvial terraces influencing its morphology – a 'threshold' deposit thickness above which subtle terrain roughness does not affect rock avalanche morphology anymore has as of yet not been determined, but might be of the order of a few to less than 10–20 m.

Emplacement mechanics

Morphological evidence at Tschirgant shows that two different modes of emplacement can occur simultaneously in the same rockslope failure event: rock sliding and rock avalanche spreading. The term 'rockslide–rock avalanche' previously implied a succession of an initial rockslide which transforms into a rock avalanche at some early point during emplacement (Hsü, 1975; Cruden and Varnes, 1996; Erismann and Abele, 2001). At Tschirgant, however, this transition is located further down the runout path. Right in the centre of the deposit, the rockslide is preserved as large, coherent hummocks. Longitudinal ridges on the central rockslide part of the Tschirgant deposit point straight back to source, thus these sliding blocks followed the initial failure trajectory. Only the left-lateral (i.e. towards the broad Inn valley) rockslide hummocks diverge from this trajectory, indicating the beginning of lateral spreading. All longitudinal ridges on the rock avalanche part, however, document radial spreading of a morphologically more disintegrated mass; i.e. more and smaller hummocks. Fewer megablocks per unit area on the rock avalanche, but identical relative distribution of megablocks (inset Figure 10) on both, the rockslide and the rock avalanche, suggest that breakage in the carapace is equal and passive for both emplacement modes (i.e. spreading versus *en masse* sliding). The difference in megablock density distributions simply reflects the differences in degree of spreading (i.e. hummock size and separation).

Lithologic control

The observation that source stratigraphy is preserved in the deposit (Heim, 1932; Hadley, 1964; Hewitt, 1988; Abbott *et al.*, 2002; Hewitt *et al.*, 2008; this study) establishes that rock avalanches (and, of course, rockslides) move in a predominantly laminar fashion, categorically excluding mixing. Hence, granular 'flows' are dry (i.e. unsaturated), frictional, grain–contact–dependent systems (Straub, 1997; Davies, 1982; Legros, 2002). Preservation of the lithological order in all areas of the Tschirgant deposit, despite long runout, strong topographic interference, and intensive crushing puts further emphasize on the lack of mixing.

Lithology, in this context the dynamic geomechanical characteristics of the rock mass, seems to impart the strongest control on deposit morphology. At Tschirgant, each lithology has its own distinct deposit morphology (Figure 13), which, after initial classification in the field, can be readily identified on LiDAR imagery. High hummocks and ridges form in the competent Wetterstein carbonates (featuring megablocks), gentle topography in the weak and highly sheared Raibl rauhwacken (no megablocks), blockfields dominated by 0.5 m-sized boulders in Hauptdolomit, and a particular rugged terrain is made up of disrupted gneiss-boulder deposits. The Wetterstein Fm is predisposed to forming larger blocks because of thicker beds in these units. Hauptdolomit is commonly well-stratified, so blocks up to the metre-range are encountered, with the rare exception of larger ones. It is interesting to note that even though the Raibl beds are not capable of forming high ridges, clayshale offsets (Figure 9) along inferred lines that coincide with the local spreading direction indicate that radial spreading and lobe formation also occurred in this lithology. Furthermore, the initial slope collapse was very likely mechanically favoured by the presence of the weak Raibl beds at the toe of the slope.

More detailed case studies are necessary to test whether these findings are valid in other lithologies as well. To our knowledge, no previous studies have addressed the role of lithology and source predisposition in shaping rock avalanche deposit surfaces. Some studies make peripheral mention of lithological distribution, or evidence for differences in morphological expressions can be recognized in their presented field photographs. Roberts and Evans (2013), for example, studied the gigantic Saidmarreh rock avalanche in Iran. In their figure 14, we identified lithologic control on deposit morphology: competent limestones from the upper 'stack' of slope–parallel–dipping sequences form the distal deposit with very large blocks, whereas the adjacent medial deposit of interbedded sequences (shaly, less competent, clayey/argillaceous limestones, calcareous shales and marls) contrasts with much smaller hummocks of apparently more crushed material. This is strikingly similar to our observations at Tschirgant and supports our emphasis of a strong lithologic control on rock avalanche morphology.

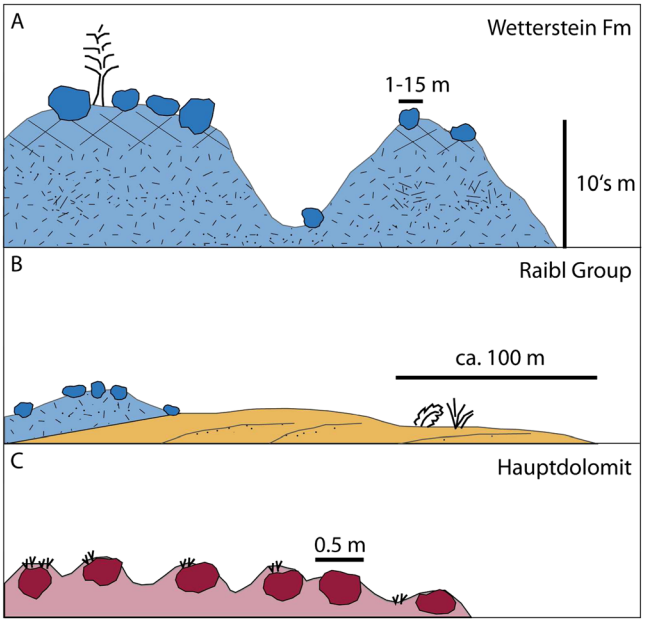

Figure 13. Relationship between lithology and deposit thickness, hummock height, and surface block sizes. This figure is available in colour online at wileyonlinelibrary.com/journal/espl

Conclusions

Notable findings presented in this paper focus on the link between deposit characteristics and emplacement processes. By this detailed study of the Tschirgant rockslide – rock avalanche deposit (its elaborate descriptions inspired by exemplary work on volcanic mass movements), we have systematically investigated the factors that shape the morphology of the final deposit. Despite the apparent complexity of rock avalanches, several fundamental processes and features can be identified. Specific interrelations of processes and properties at Tschirgant include these most striking findings and interrelationships:

- *Substrate interactions*. Substrates shape rock avalanche morphology and highlight internal/basal rock avalanche deformation (e.g. faults) by providing visual markers.
- *Topographic interference*. Even though runout path topography induces considerable complexities, our observations suggest that the intrinsic, dynamic, and lithological properties of the streaming debris are the main controls on the resulting deposit morphology.
- *Emplacement mechanics*. Two different emplacement modes are present in the same event: linear rock sliding and radial rock avalanche spreading. Megablock distribution density is a function of the different degrees of spreading in the two depositional areas, whereas identical megablock sizes in both areas suggests passive carapace breakage.
- *Intrinsic dynamics of granular materials*. Tendencies for radial alignments and longitudinal ridge formation are present in all accumulation areas. Their specific development, however, is strongly controlled by lithology.
- *Lithologic control*. The lithological distribution in the final deposit indicates radial spreading. Source structural setting predetermines maximum megablock sizes. Each lithology has its own unique deposit morphology; yet all of them show the signs of intrinsic tendencies of all granular materials. Hummock and ridge sizes are correlated strongly with lithology (for some, morphological expressions of ridge/lobe formation may be absent, yet can be traced in structural offsets of marker beds).

These findings are of significance to better understanding the process–landform relationships of rock avalanches. Recognition of such fundamental processes is relevant to interpretations of the degree and causal factors of complexity, for a more complete understanding of emplacement processes, and for assessing the validity of numerical and theoretical emplacement models. Future research should put strong focus on the influence that different lithologies have on rock avalanche emplacement processes and morphology.

Acknowledgements—This research was funded by the German Research Foundation grant DU1294/2-1 to AD (project 'Long-runout landslides: the influence of lithology on comminution, (micro-)structures, morphology, and runout'). The authors acknowledge GRID-IT for taking custom aerial photographs by quadcopter. This study (C.P.) was also funded by the research project AdaptInfra, performed at alpS GmbH (Innsbruck, Austria) and supported by the TIWAG-Tiroler Wasserkraft AG, ILF Consulting Engineers and the Austrian Research Promotion Agency (COMET-programme). The authors thank the journal editor S.N. Lane, T.R. Davies and two anonymous reviewers for very constructive suggestions which helped to significantly improve the structure and clarity of this manuscript.

References

Abbott PL, Kerr DR, Stevens EB, Washburn JL, Rightmer DA. 2002. Neogene sturzström deposits, Split Mountain area, Anza-Borrego Desert State Park, California. In *Catastrophic Landslides: Effects, Occurrence, and Mechanisms*, Evans SG, DeGraff JV (eds) Geological Society of America Reviews in Engineering Geology 15. The Geological Society of America: Boulder, CO; 379–400.

Abdrakhmatov K, Strom AL. 2006. Dissected rockslide and rock avalanche deposits; Tien Shan, Kyrgyzstan. In *Landslides from Massive Rock Slope Failure*, Evans SG, Scarascia-Mugnozza G, Strom AL, Hermanns RL (eds) Nato Science Series IV, Earth and Environmental Sciences 49. NATO: Washington, DC; 551–570.

Abele G. 1972. Kinematik und Morphologie spät- und postglazialer Bergstürze in den Alpen. *Zeitschrift für Geomorphorphologie, N.F. Suppl.* **14**: 138–149.

Abele G. 1974. Bergstürze in den Alpen, ihre Verbreitung, Morphologie und Folgeerscheinungen. *Wissenschaftliche Alpensvereinshefte* **25**: 230 pp.

Abele G. 1997. Rockslide movement supported by the mobilization of groundwater-saturated valley floor sediments. *Zeitschrift für Geomorphorphologie* **41**: 1–20.

Albrich T, Gisinger A. 1992. *Im Bombenkrieg: Tirol und Vorarlberg 1943–1945*. Haymon Verlag: Innsbruck; **201–204**, 294, 339–341.

Ampferer O. 1904. Die Bergstürze am Eingang des Ötztales und am Fernpaß. *Verhandlungen der Geologischen Reichsanstalt* **1904**: 73–87.

Ampferer O. 1905. Geologische Beschreibung des Seefelder, Mieminger und südlichen Wettersteingebirges. *Jahrbuch der Geologischen Reichsanstalt* **55**(3): 451–474.

Belusov A, Belusova A, Voight B. 1999. Multiple edifice failures, debris avalanches and associated eruptions in the Holocene history of Shiveluch Volcano, Kamchatka, Russia. *Bulletin of Volcanology* **61**(5): 324–342.

Bösmeier A. 2014. Structures at the distal limit of the Tschirgant rock avalanche, Tyrol, Austria, MSc Thesis. Universität Freiburg, Freiburg; 80 pp.

Brandner R. 1980. *Geologische und Tektonische Übersichtskarte von Tirol, Tirol-Atlas, C1, C3*. Universitätsverlag Wagner: Innsbruck.

Brandner R. 1984. Meeresspiegelschwankungen und Tektonik in der Trias der NW-Tethys. *Jahrbuch der Geologischen Bubesanstalt* **126**(4): 435–475.

Brandner R, Poleschinski W. 1986. Stratigraphie und Tektonik am Kalkalpensüdrand zwischen Zirl und Seefeld in Tirol (Exkursion D am 3. April 1986). *Jahresberichte und Mittelungen des Oberrheinischen Geologischen Vereins* **68**: 67–92.

Capra L, Macías JL, Scott KM, Abrams M, Garduño-Monroy VH. 2002. Debris avalanches and debris flows transformed from collapses in the Trans-Mexican Volcanic Belt, Mexico – behavior, and implications for hazard assessment. *Journal of Volcanology and Geothermal Research* **113**(1–2): 81–110.

Clavero J, Polanco E, Godoy E, Aguilar G, Sparks RSJ, van Wyk de Vries B, de Arce CP, Matthews S. 2004. Substrata influence in the transport and emplacement mechanism of the Ollagüe debris avalanche (northern Chile). *Acta Vulcanologica* **16**(1–2): 59–76.

Clavero J, Sparks R, Huppert H, Dade W. 2002. Geological constraints on the emplacement mechanism of the Parinacota debris avalanche, northern Chile. *Bulletin of Volcanology* **64**(1): 40–54.

Cruden DM, Varnes DJ. 1996. Landslide types and processes. In *Landslides: Investigation and Mitigation*, Turner AK, Schuster LR (eds). Transportation Research Board Special Report, Vol. **247**; 36–75.

Davies TR. 1982. Spreading of rock avalanche debris by mechanical fluidization. In *Rock Mechanics*, Vol. **15**; 9–24.

Davies TR, McSaveney MJ. 2012. Mobility of long-runout rock avalanches. In *Landslides – Types, Mechanisms and Modeling*, Clague JJ, Stead D (eds). Cambridge University Press: Cambridge; 50–59.

Donofrio DA, Brandner R, Poleschinski W. 2003. Conodonten der Seefeld-Formation: Ein Beitrag zur Bio- und Lithostratigraphie der Hauptdolomit-Plattform (Obertrias, Westliche Nördliche Kalkalpen, Tirol). *Geologisch-Paläontologische Mitteilungen Innsbruck* **26**: 91–107.

Dufresne A. 2009. Influence of Runout Path Material on Rock and Debris Avalanche Mobility: Field Evidence and Analogue Modeling, PhD Thesis. University of Canterbury, Christchurch, New Zealand; 271 pp.

Dufresne A. 2012. Granular flow experiments on the interaction with stationary runout path materials and comparison to rock avalanche events. *Earth Surface Processes and Landforms* **37**: 1527–1541.

Dufresne A, Davies TR. 2009. Longitudinal ridges in mass movement deposits. *Geomorphology* **105**: 171–181.

Dufresne A, Davies TR, McSaveney MJ. 2009. Influence of runout-path material on emplacement of the Round Top rock avalanche, New Zealand. *Earth Surface Processes and Landforms* **35**: 190–201.

Dufresne A, Prager C, Clague JJ. 2014. Complex interactions of rock avalanche emplacement with fluvial sediments: field structures at the Tschirgant deposit, Austria. In *Engineering Geology for Society and Territory*, Lollino G, Giordan D, Crosta GB, Corominas J, Azzam R, Wasowski J, Sciarra N (eds). Springer: Berlin; volume **2**, 1707–1711.

Dufresne A, Salinas S, Siebe C. 2010. Substrate deformation associated with the Jocotitlán edifice collapse and debris avalanche deposit, central Mexico. *Journal of Volcanology and Geothermal Research* **197**: 133–148.

Eisbacher GH, Brandner R. 1995. Role of high-angle faults during heteroaxial contraction, Inntal Thrust Sheet, Northern Calcareous Alps, Western Austria. *Geologisch-Paläontologische Mitteilungen Innsbruck* **20**: 389–406.

Ekström G, Stark CP. 2013. Simple scaling of catastrophic landslide dynamics. *Science* **339**(6126): 1416–1419.

Erismann TH, Abele G. 2001. *Dynamics of Rockslides and Rockfalls*. Springer: Heidelberg; 316 pp.

Fort M. 1996. Late Cenozoic environmental changes and uplift of the northern side of the Central Himalaya: a reappraisal from field data. *Palaeogeography, Palaeoclimatology, Palaeoecology* **120**: 123–145.

Fruth I, Scherreiks R. 1982. Hauptdolomit (Norian) – stratigraphy, paleogeography and diagenesis. *Sedimentary Geology* **32**: 195–231.

Geertsema M, Hungr O, Schwab JW, Evans SG. 2006. A large rockslide-debris avalanche in cohesive soil at Pink Mountain, northeastern British Columbia, Canada. *Engineering Geology* **83**: 64–75.

Geofast. 2011. Zusammenstellung ausgewählter Archivunterlagen der Geologischen Bundesanstalt, Blatt 116 – Telfs (Ausgabe 2011/04), 145 – Imst (Ausgabe 2011/07), 146 – Oetz (Ausgabe 2011/07), 1:50.000. Geologische Bundesanstalt: Wien.

Glicken H. 1996. *Rockslide–Debris Avalanche of May 18, 1980, Mount St. Helens, Washington*USGS Open-file Report 96-677. US Geological Survey: Reston, VA; 90 pp.

Goldberger J. 1947. Karsterscheinungen, Buckelwiesen und Bergzerreissungsformen am Tschirgant, Unpublished Hausarbeit. University Innsbruck.

Goldberger J. 1950. Morphologische Beobachtungen am Tschirgant bei Imst. *Schlern-Schriften* **65**: 9–17.

Grottenthaler W. 1968. Zur Geologie des Tschirgant zwischen Gurgltal im Norden und dem Kalkalpensüdrand (Tirol), Diploma Thesis. University of Munich.

Hadley JB. 1964. *Landslides and Related Phenomena Accompanying the Hebgen Lake Earthquake of August 17, 1959*USGS Professional Paper 435-K. US Geological Survey: Reston, VA; 107–138.

Hancox GT, Perrin ND. 1994. Green Lake landslide: a very large ancient rock slide in Fiordland, New Zealand. *Proceedings of the 7th IAEG Congress, Lisbon, 5*–9 September; volume **3**, 1677–1689.

Hartleitner K. 1993. Die Planung der 'Neuen Bahn' im Abschnitt Ötztal-Landeck: Geologische Ergebnisse. In *Arbeitstagung 1993 Geologischen Bundesanstalt, Geologie des Oberinntaler Raumes, Schwerpunkt Blatt 144 Landeck*, Hauser C, Nowotny A (eds). Geologische Bundesanstalt: Wien; 139–140.

Heim A. 1932. *Bergsturz und Menschenleben [Landslides and human lives]*Vierteljahrsschrift der Naturforschenden Gesellschaft in Zürich, 77. Beer & Co. in Komm: Zürich; 218 pp.

Heuberger H. 1966. Gletschergeschichtliche Untersuchungen in den Zentralalpen zwischen Sellrain- und Ötztal. *Wissenschaftliche Alpenvereinshefte* **20**: 125.

Heuberger H. 1975. Das Ötztal. Bergstürze und alte Gletscherstände, kulturgeographische Gliederung. In *Innsbrucker Geographische Studien **2** (Exkursionsführer Tirol)*. Geographie Innsbruck; 213–249.

Hewitt K. 1988. Catastrophic landslide deposits in the Karakoram Himalaya. *Sciences* **242**: 64–67.

Hewitt K. 1999. Quaternary moraines vs catastrophic rock avalanches in the Karakoram Himalaya, northern Pakistan. *Quaternary Research* **51**(3): 220–237.

Hewitt K. 2002. Styles of rock-avalanche depositional complexes conditioned by very rugged terrain, Karakoram Himalaya, Pakistan. *Reviews in Engineering Geology* **15**: 345–377.

Hewitt K, Clague JJ, Orwin JF. 2008. Legacies of catastrophic rock slope failures in mountain landscapes. *Earth-Science Reviews* **87**: 1–38.

Hsü K. 1975. Catastrophic debris streams (sturzstroms) generated by rockfalls. *GSA Bulletin* **86**: 129–140.

1Hungr O, Evans SG. 2004. Entrainment of debris in rock avalanches: an analysis of a long run-out mechanism. *GSA Bulletin* **116**: 1240–1252.

Hutchinson JN, Bhandari RK. 1971. Undrained loading; a fundamental mechanism of mudflows and other mass movements. *Geotechnique* **21**: 353–358.

Indlekofer J. 2014. Karst oder Konflikt an der Inn-Ötztaler Ache Mündung, Tirol, BSc Thesis. Universität Freiburg, Germany; 44 pp.

Jibson RW, Harp EL, Schulz W, Keefer DK. 2006. Large rock avalanches triggered by the M 7.9 Denali fault, Alaska, earthquake of 3 November 2002. *Engineering Geology* **83**: 144–160.

Johnson B. 1978. Blackhawk landslide, California, US. In *Rockslides and Avalanches: Natural Phenomena 1 (Developments in Geotechnical Engineering)*, Voight B (ed). Elsevier: Amsterdam; 481–504.

Kamata H, Mimura K. 1983. Flow directions inferred from imbrication in the Handa pyroclastic flow deposit in Japan. *Bulletin of Volcanology* **46**(3): 277–282.

Kelfoun K, Druitt T, van Wyk de Vries B, Guilbaud M-N. 2008. Topographic reflection of the Socompa debris avalanche, Chile. *Bulletin of Volcanology* **70**(10): 1169–1187.

Legros F. 2002. The mobility of long-runout landslides. *Engineering Geology* **63**: 301–331.

Mair P. 1997. Die Föhrenwälder der Bergsturzgebiete Tschirgant und Köfels (Tirol), Diploma Thesis. University of Innsbruck, Austria; 163 pp.

Mahoney KA. 2013. *Fifteenth Air Force against the Axis: Combat Missions over Europe during World War II*. Scarecrow Press: Plymouth; **390–394.**

McColl ST, Davies TR. 2011. Evidence for a rock-avalanche origin for 'The Hillocks' 'moraine', Otago, New Zealand. *Geomorphology* **127**: 216–224.

McSaveney MJ. 1978. Sherman Glacier rock avalanche, Alaska, USA. In *Rockslides and avalanches: Natural Phenomena 1 (Developments in Geotechnical Engineering)*, Voight B (ed.). Elsevier: Amsterdam; 197–258.

Naranjo JA, Francis P. 1987. High velocity debris avalanche at Lastarria volcano in the north Chilean Andes. *Bulletin of Volcanology* **49**: 509–514.

Nicoletti PG, Sorriso-Valvo M. 1991. Geomorphic controls of the shape and mobility of rock avalanches. *Geological Society of America Bulletin* **103**: 1365–1373.

Niederbacher P. 1982. Geologisch-tektonische Untersuchungen in den südöstlichen Lechtaler Alpen (Nördliche Kalkalpen, Tirol). *Geologisch-Paläontologische Mitteilungen Innsbruck* **12**(7): 123–154.

Ostermann M, Ivy-Ochs S, Sanders D, Prager C, Patzelt G. (n.d). Submitted for publication. Multi-method approach (234U/230Th, 36Cl, 14C) to age-date a catastrophic rock slope failure,): problems and prospect in age determination of mass-wasting (Tschirgant, Eastern Alps, Austria). Earth Surface Processes and Landforms.

Ostermann M, Prager C. 2014. Major Holocene rock slope failures in the Upper Inn-Ötz valley region (Tyrol, Austria). In *From the Foreland to the Central Alps*, Kerschner H, Krainer K, Spötl C (eds). DEUQUA Excursions. Geozon: Berlin; 116–126.

Ostermann M, Sanders D. 2009. Proxy-dating the Tschirgant rockslide event with the U/Th method. *Geophysical Research Abstracts* **12**: EGU2010-24-1.

Ostermann M, Sanders D, Ivy-Ochs S, Alfimov V, Rockenschaub M, Römer A. 2012. Early Holocene (8.6 ka) rock avalanche deposits, Obernberg valles (eastern Alps): landform interpretation and kinematics of rapid mass movement. *Geomorphology* **171–172**: 83–93.

Pagliarini L. 2008. *Strukturelle Neubearbeitung des Tschirgant und Analyse der lithologisch-strukturell induzierten Massenbewegung (Tschirgant Bergsturz, Nördliche Kalkalpen, Tirol)*, Diploma Thesis. Universität Innsbruck, Austria; 89 pp.

Paguican EMR, van Wyk de Vries B, Lagmay A. 2014. Hummocks: how they form and how they evolve in rockslide-debris avalanches. *Landslides* **11**: 67–80.

Patzelt G. 2012. The rock avalanches of Tschirgant and Haiming (Upper Inn Valley, Tyrol, Austria), comment on the map supply. *Jahrbuch der Geologischen Bundesanstalt* **152**(1–4): 13–24.

Patzelt G, Poscher G. 1993. Der Tschirgant Bergsturz. *Arbeitstagung 1993 der Geologischen Bundesanstalt – Geologie des Oberinntaler Raums* 208–213.

Pavoni N. 1968. Über die Entstehung der Kiesmassen im Bergsturzgebiet von Bonaduz-Reichenau (Graubünden). *Eclogae Geologicae Helvetiae* **61**: 494–500.

Pouliquen O, Delour J, Savage SB. 1997. Fingering in granular flows. *Nature* **386**: 816–817.

Prager C. 2010. *Geologie, Alter und Struktur des Fernpass Bergsturzes und tiefgründiger Massenbewegungen in seiner Umgebung (Tirol, Österreich)*, PhD Thesis. Universität Innsbruck, Austria; 307 pp.

Prager C, Ivy-Ochs S, Ostermann M, Synal H-A, Patzelt G. 2009. Geology and radiometric 14C, 36Cl- and Th-/U-dating of the Fernpass rockslide (Tyrol, Austria). *Geomorphology* **103**(1): 93–103.

Prager C, Krainer K, Seidl V, Chwatal W. 2006. Spatial features of Holocene Sturzstrom-deposits inferred from subsurface investigations (Fernpass rockslide, Tyrol, Austria). *GeoAlp* **3**: 147–166.

Prager C, Pagliarini L, Brandner R. 2007. Der Tschirgant Bergsturz (Nördliche Kalkalpen, Tirol, Österreich): prominentes Fallbeispiel einer lithologisch und strukturell prädisponierten Felsgleitung. *GeoAlp* **4**: 74.

Prager C, Zangerl C, Kerschner H. 2012. Sedimentology and mechanics of major rock avalanches: implications from (pre-) historic Sturzstrom deposits (Tyrolean Alps, Austria). In *Landslides and Engineered Slopes: Protecting Society through Improved Understanding*, Eberhardt E, Froese C, Turner K, Leroueil S (eds). Taylor & Francis Group: London; 895–900.

Prager C, Zangerl C, Patzelt G, Brandner R. 2008. Age distribution of fossil landslides in the Tyrol (Austria) and its surrounding areas. *Natural Hazards and Earth System Sciences* **8**: 377–407.

Probst G, Brandner R, Hacker P, Heiss G, Prager C. 2003. Hydrogeologische Grundlagenstudie Westliche Gailtaler Alpen / Lienzer Dolomiten (Kärnten/Osttirol). *Steirische Beiträge zur Hydrogeologie* **54**: 5–62.

Richter E. 2010. *Neubau der Ötztaler Achbrücke: kampfmittelsicherheitstechnische Maßnahmen*, Vol. **3–33**. ÖBB Infrastruktur AG: Wien.

Roberts NJ, Evans SG. 2013. The gigantic Seymareh (Saidmarreh) rock avalanche, Zagros Fold-Thrust Belt, Iran. *Journal of the Geological Society, London* **170**: 685–700.

Robinson TR, Davies TR, Reznichenko NV, De Pascale GP. 2014. The extremely long-runout Komansu rock avalanche in the Trans Alai range, Pamir Mountains, southern Kyrgyzstan. *Landslides* **12**(3): 523–535.

Sanders D, Ostermann M, Brandner R, Prager C. 2010. Meteoric lithification of catastrophic rockslide deposits: diagenesis and significance. *Sedimentary Geology* **223**(1–2): 150–161.

Shea T, van Wyk de Vries B. 2008. Structural analysis and analogue modeling of the kinematics and dynamics of rockslide avalanches. *Geosphere* **4**(4): 657–686.

Siebert L. 2002. Landslides resulting from structural failure of volcanoes. *GSA Reviews in Engineering Geology* **15**: 209–235.

Smith GM, Davies TR, McSaveney MJ, Bell DH. 2006. The Acheron rock avalanche, Canterbury, New Zealand – morphology and dynamics. *Landslides* **3**: 62–72.

Sørensen S-A, Bauer B. 2003. On the dynamics of the Köfels Sturzstrom. *Geomorphology* **54**: 11–19.

Straub S. 1997. Predictability of long runout landslide motion: implications from granular flow mechanics. *Geologische Rundschau* **86**(2): 415–425.

Tollmann A. 1976. *Analyse des klassischen Nordalpinen Mesozoikums. Stratigraphie, Fauna und Fazies der Nördlichen Kalkalpen*. Deuticke: Wien; 580 pp.

Unterrichter L. 1949. *Die Luftangriffe auf Nordtirol im Kriege 1939–1945*, Vol. **27**. Universitäts-Verlag Wagner: Innsbruck; **27**: 555–581.

Vallance JW, Siebert L, Rose WI, Jr, Girón JR, Banks NG. 1995. Edifice collapse and related hazards in Guatemala. *Journal of Volcanology and Geothermal Research* **66**(1–4): 337–355.

Van Asch TW, Xu W, Dong XJ. 2015. Unravelling the multiphase runout conditions of a slide-flow mass movement. *Geomorphology* **230**(1): 161–170.

Von Poschinger A. 2002. Large rockslides in the Alps: a commentary on the contribution of G. Abele (1937–1994) and a review of some recent developments. In *Catastrophic Landslides: Effects, Occurrence, and Mechanisms*, Evans SG, DeGraff JV (eds) Geological Society of America Reviews in Engineering Geology, Vol. **15**. Geological Society of America: Boulder, CO; 237–256.

Von Poschinger A, Kippel T. 2009. Alluvial deposits liquefied by the Flims rockslide. *Geomorphology* **103**: 50–56.

Weber L. 1997. Handbuch der Lagerstätten, der Erze. In *Archiv für Lagerstättenforschung 19*Industrieminerale und Energierohstoffe Österreichs. Geologischen Bundesanstalt: Wien; 607 pp.

Weichert D, Horner RB, Evans SG. 1994. Seismic signatures of landslides: The 1990 Brenda Mine collapse and the 1965 Hope rockslides. *Bulletin of the Seismological Society of America* **84**(5): 1523–1532.

Weidinger JT, Korup O, Munack H, Altenberger U, Dunning SA, Tippelt G, Lottermoser W. 2014. Giant rockslide from the inside. *Earth and Planetary Science Letters* **389**: 62–73.

Xu Q, Shang Y, van Asch T, Wand S, Zhang Z, Dong X. 2012. Observations from the large, rapid Qigong rock slide – debris avalanche, southeast Tibet. *Canadian Geotechnical Journal* **49**: 589–606.

Yarnold JC, Lombard JP. 1989. Facies model for large rock avalanche deposits formed in dry climates. In *Field Trip Guidebook – Pacific Section 62*, Colburn IP, Abbott PL, Minch J (eds). Society of Economic Palaeontologists and Mineralogists: Tulsa, OK; 9–31.

Yoshida H, Sugai T, Ohmori H. 2012. Size–distance relationships for hummocks on volcanic rockslide-debris avalanche deposits in Japan. *Geomorphology* **136**(1): 76–87.

Supporting Information

Additional supporting information may be found in the online version of this article at the publisher's web site